PCCP

Accepted Manuscript

ROYAL SOCIETY OF CHEMISTRY

www.rsc.org/pccp

A Comparative Study of Ru (II) Cyclometallated Versus Thiocyanated Heteroleptic Complexes: Thermodynamic Force for Efficient Dye Regeneration in Dye-sensitized Solar Cells and How Low Could it Be?

Maqbool Hussain[a], Ashraful Islam[b]*, Idriss Bedja[c], Ravindra Kumar Gupta[c], Liyuan Han[b], Ahmed El-Shafei[a]*
[1]Polymer and Color Chemistry Program, North Carolina State University, Raleigh, NC, 27695, USA

[b]*Photovoltaic Materials Unit, National Institute for Materials Science, 1-2-1 Sengen, Tsukuba, Ibaraki 305-0047, Japan, (ISLAM.Ashraful@nims.go.jp)*

[c]*CRC, Optometry Department, College of Applied Medical Sciences, King Saud University, Riyadh 11433, Saudi Arabia*

*Corresponding author: Ahmed_El-Shafei@ncsu.edu

Abstract

Four novel Ru (II) bipyridyl complexes **MH12-15** were synthesized and characterized for dye-sensitized solar cells (DSSCs). Their photovoltaic performance including incident photon-to-current conversion efficiency (IPCE), total solar-to-power conversion efficiency ($\eta\%$) and ground and excited states oxidation potentials and photoelectrochemical properties were evaluated on mesoporous nanocrystalline TiO_2 and compared with the benchmark N719-Dye under the same experimental condition. **MH12-15** showed stronger MLCT with significantly higher molar extinction coefficient at the lower energy absorption of 553nm (27,500 $M^{-1}cm^{-1}$), 554nm (34,605 $M^{-1}cm^{-1}$) and 577nm (23,300 $M^{-1}cm^{-1}$), and 582nm (39,000 $M^{-1}cm^{-1}$) than that of **N719** (14,200 $M^{-1}cm^{-1}$). Introduction of cyclometallated ligand in dyes **MH14-15** improved the optical properties and red-shift of 24nm and 28nm, respectively, compared to the non-cyclometallated analogs **MH12-13.** The red shift in UV-Vis spectra of **MH14-15** can be attributed to the destabilization of the HOMO t_2g of Ru (II). However, the destabilization of the HOMO furnished upward shift of the ground state oxidation potentials (GSOP) of **MH14-15** at -5.44 eV and -5.36 eV against *vacuum*, respectively, which resulted in a driving force of only 0.22 and 0.16eV for dyes **MH14-15** regeneration, respectively. In the case of NCS analogs, MH12-13, the GSOPs, however, were -5.56 and -5.51 eV, respectively, which produced driving force of more than 0.25eV for dye regeneration. Nanosecond transient absorbance measurements showed that the time needed for the oxidized forms of **MH12-MH15** to

regenerate the neutral dye is 6 μs, 4 μs, 13 μs and 18 μs, respectively, compared to N719 (2.3 μs). These kinetics data confirmed that the weak thermodynamic force, small negative free energy (-ΔG), for neutral dye regeneration of **MH14-15** makes the dye regeneration process kinetically sluggish, which contributed significantly to the loss of both photocurrent and photovoltage. This study clearly elucidated that although cyclometallation may produce significantly better light harvesting, the driving force of less than 0.25 eV is not sufficiently enough for effective dye regeneration.

Keywords: Dye-sensitized solar cells, cyclometallated complexes, solar-to-power conversion efficiency, IPCE, ground and excited state potentials and Ru (II) bipyridyl complexes.

1. **Introduction**

The use of photovoltaic devices has increased in popularity as an alternative method to generate electricity from the sunlight. These devices function by converting solar photons into useful electrons through photoelectrochemical process and ultimately produce photocurrent. Currently, the majority of photovoltaic cells are based on silicon because of their suitable physical and chemical properties. However, the main issue with these cells is the expensive processing cost to produce the pure silicon needed for optimum solar cell efficiency. Due to the high cost of production, silicon cells are limited in its ability to compete with fossil fuels and the emerging new PV technologies. Dye-sensitized solar cells (DSSCs) are considered as a potential alternative to traditional silicon solar cells because of their cost-effective solar-to-power conversion efficiency. [1-2] So far the best performances in terms of solar-to-power conversion efficiency are shown by Ru (II) polypyridyl sensitizers [3-4] attributed to their strong metal-to-ligand charge transfer (MLCT) properties [5-10], rich fluorescence behavior, stable ground and excited states potentials, and long excited state life time [11-14]. However, most of the Ru (II) polypyridyl complexes show MLCT absorption in a narrow range of the solar spectrum, typically 400 nm and 600 nm. In addition, the benchmark Ru (II) polypyridyl complex, known as N719, contains labile thiocynonato (-NCS) ligand which is unstable towards light, and it decomposes over time, which leads to a considerable loss in the device efficiency. [15] Preferably, a sensitizer must be stable towards light and temperature [16] at least for 20 years without significant loss of performance corresponding to a 50-100 millions turnover of electron transfer reactions. [17] Many attempts have been reported to replace these fragile ligands in order to increase the stability of

DSSCs. Most recently, Barigelletti and co-workers reported several Ru (II) cyclometallated complexes that offers opportunity to circumvent the labile thiocynonato (-NCS) ligand and showed promising stability for dye-sensitized solar cells.[18-19] A common approach for replacing –NCS group is using cyclometallating ligands that increases the stability of solar device, which also allows for fine tuning of the ground and excited state oxidation potentials, which may translates into higher conversion efficiency and better performance stability of DSSCs. This strategy was first demonstrated by Koten and co-workers by developing a tridentate cyclometallated complexes, and they were able to achieve maximum incident photon-to-current conversion efficiency (IPCE) of 70% around 550 nm.[20] Later, in 2009, Gräetzel and co-workers used similar approach and developed a novel Ru (II) cyclometallated complex that exhibited a remarkable overall conversion efficiency of 10.1% and IPCE efficiency of 83%. To date several cyclometallated complexes are reported in the literature that exhibits more than overall conversion efficiency of the benchmark dye (*i.e.,* $\eta > 10\ \%$) [21-23 13].

Polypyridyl cyclometallated complexes consist of a central ruthenium (II) with ancillary light harvesting ligand and anchoring groups and one cyclometallated ligand. Figure 1 shows one of the novel cyclometallated Ru (II) bipyridyl complex we developed recently in our laboratory and the principle mode of operation including sensitization and charge-injection from the dye into the conduction band of TO_2.

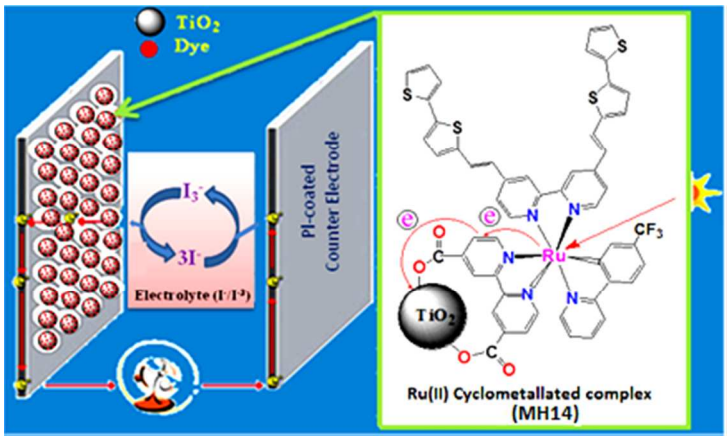

Figure 1: A schematic diagram of photo-induced metal-to-ligand charge transfer (MLCT) transition and current flow in DSSC by using Ru (II) bipyridyl cyclometallated complexes (MH14), TiO_2 as semiconductor and iodine/iodide (I^-/I^{-3}) as electrolyte.

Further advancement of cyclometallated complex, however, demands better understandings at the molecular level to enhance the performance of DSSCs. With this in mind, we designed and developed four novel sensitizers coded **MH12-15**. **MH12-13** contains labile thiocynonato (-NCS) ligand and in **MH14-15** the -NCS ligand is substituted by 2-(4-trifluoromethyl-phenyl)-pyridine cyclometallated ligand while maintaining the same ancillary ligands of bithiophene and terthiophene stilbazole-based. The incorporation of additional thiophene unit enhanced the molar extinction coefficient for both the π→π* and 4d→π* MLCT transition. In addition, the high molar extinction coefficient offers the great benefit of reducing the amount of dye loading and film thickness of TiO_2, which opens the door for high efficiency translucent DSSCs. The better light harvesting properties and the use of thinner layers of TiO_2 facilitates more charge collection and a reduction in dark current, which translates into higher open-circuit photovoltage.[31] The molecular structures of **MH12-MH15** are shown in Figure 2.

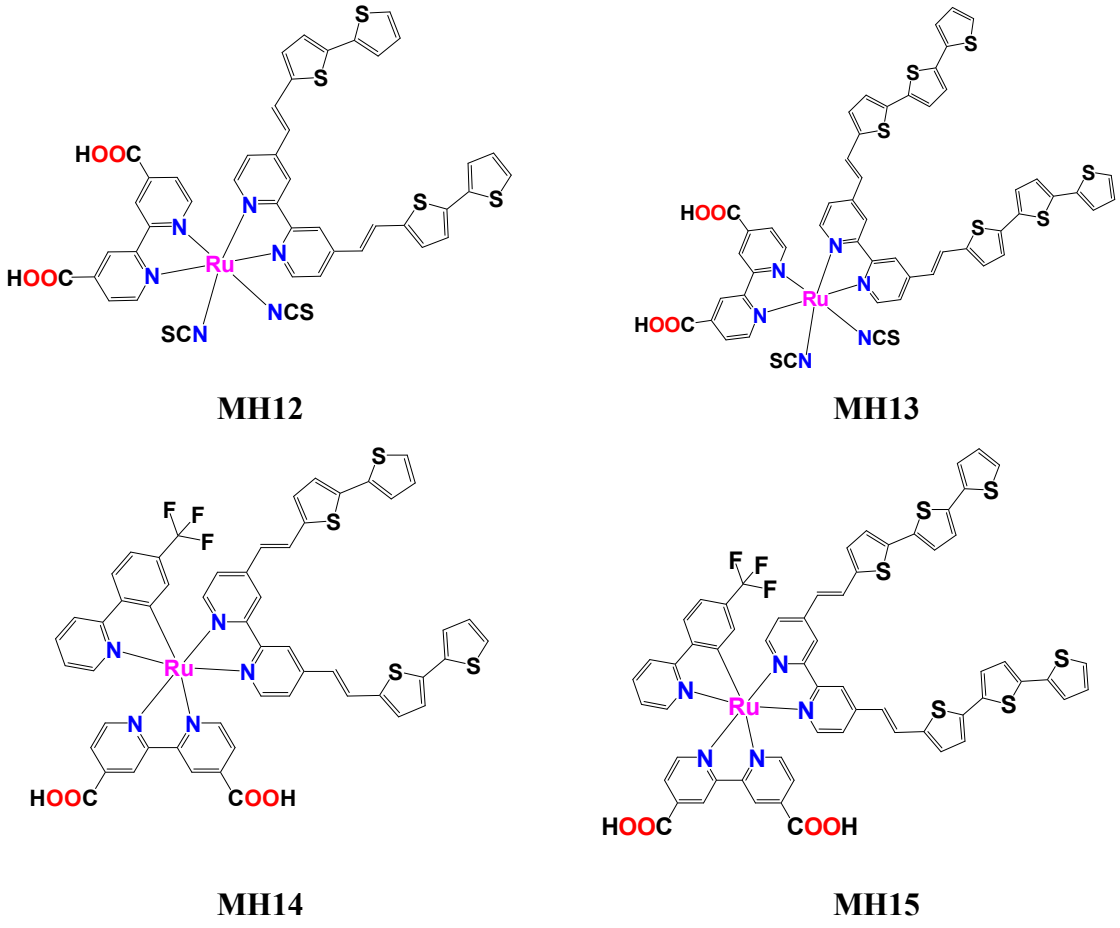

Figure 2: Molecular structures of complexes **MH12-15.**

2. Experimental Section

2.1. Synthesis of Ru (II) bipyridyl complexes

The solvents and chemicals were either purchased from Sigma-Aldrich, Fisher Scientific or TCI-America and used as received. Sephadex LH-20 was purchased from Fisher Scientific. The synthesis of all ligands and complexes were prepared using modified published procedures. Complexes **MH12-13** was synthesized according to our previously published procedure [26] details were provided in the supporting information.

Ru (II) [cis(4,4'-Bis-(2-[2,2']bithiophenyl-5-yl-vinyl)-bis[2,2'] bipyridinyl-2, 2'-bipyridinyl-4, 4'-dicarboxylic-(2-(2-(4-Trifluoromethyl-phenyl)-pyridine)] (MH14) complex were synthesized in dark under argon atmosphere. In a 250 ml reaction flask dichloro-(*p*-cymene)-ruthenium (II) dimer (0.556g, 9.08 x 10^{-4} mol) and 2-(4-Trifluoromethyl-phenyl)-pyridine (0.406g, 1.816 x 10^{-3} mol) was dissolved in 100 mL of MeCN and then NaOH (0.073g, 1.816 x 10^{-3} mol) and KPF_6 (0.670g, 3.638 x 10^{-3} mol) was added to the stirring solution. The reaction mixture was stirred at 45 °C for 45h. The MeCN was removed from reaction mixture using a rotary evaporator and collected yellow-greenish product which is purified by column chromatography using silica gel as the stationary phase and mixture of $CH_2Cl_2$and MeCN (98:2) as the mobile phase.

In the second step a 250 mL fask was charged with [C^N)Ru $(CH_3CN)_4$ (2-(4-Trifluoromethyl-phenyl)-pyridine)]$^+PF_6^-$ (0.400g, 6.324 x 10^{-4} mol) and 4,4'-Bis-(2-[2,2']bithiophenyl-5-yl-vinyl)-[2,2']bipyridinyl (0.339g, 6.324 x 10^{-4} mol) using DMF, C_2H_5OH mixture (100 mL, 3:2). The reaction mixture was stirred for 2h at 70 °C and then increased the temperature to 90°C and added [2,2']Bipyridinyl-4,4'-dicarboxylic acid diethyl ester (0.190g, 6.324 x 10^{-4} mol) and stirred for further 2h under nitrogen. The DMF, C_2H_5OH mixture was removed from reaction mixture using a rotary evaporator. De-ionized water was added to flak and neutralized using 0.01M HNO_3 to Ph 7.03. The green product filtered and purified by column chromatography, using Sephadex LH-20 as the stationary phase and pure methanol as the mobile phase and collected green product. The purified product was hydrolyzed by refluxing for 48h at 100 °C in DMF, H_2O and Triethylamine (50 ml, 3:1:1) the insoluble solid were vacuum filtered and washed with de-ionized water and ether. The product was dried overnight to give 80% yield with respect to the [C^N)Ru $(CH_3CN)_4$ (2-(4-Trifluoromethyl-phenyl)-pyridine)]$^+PF_6^-$ intermediate, overall synthesis is shown in scheme 1.

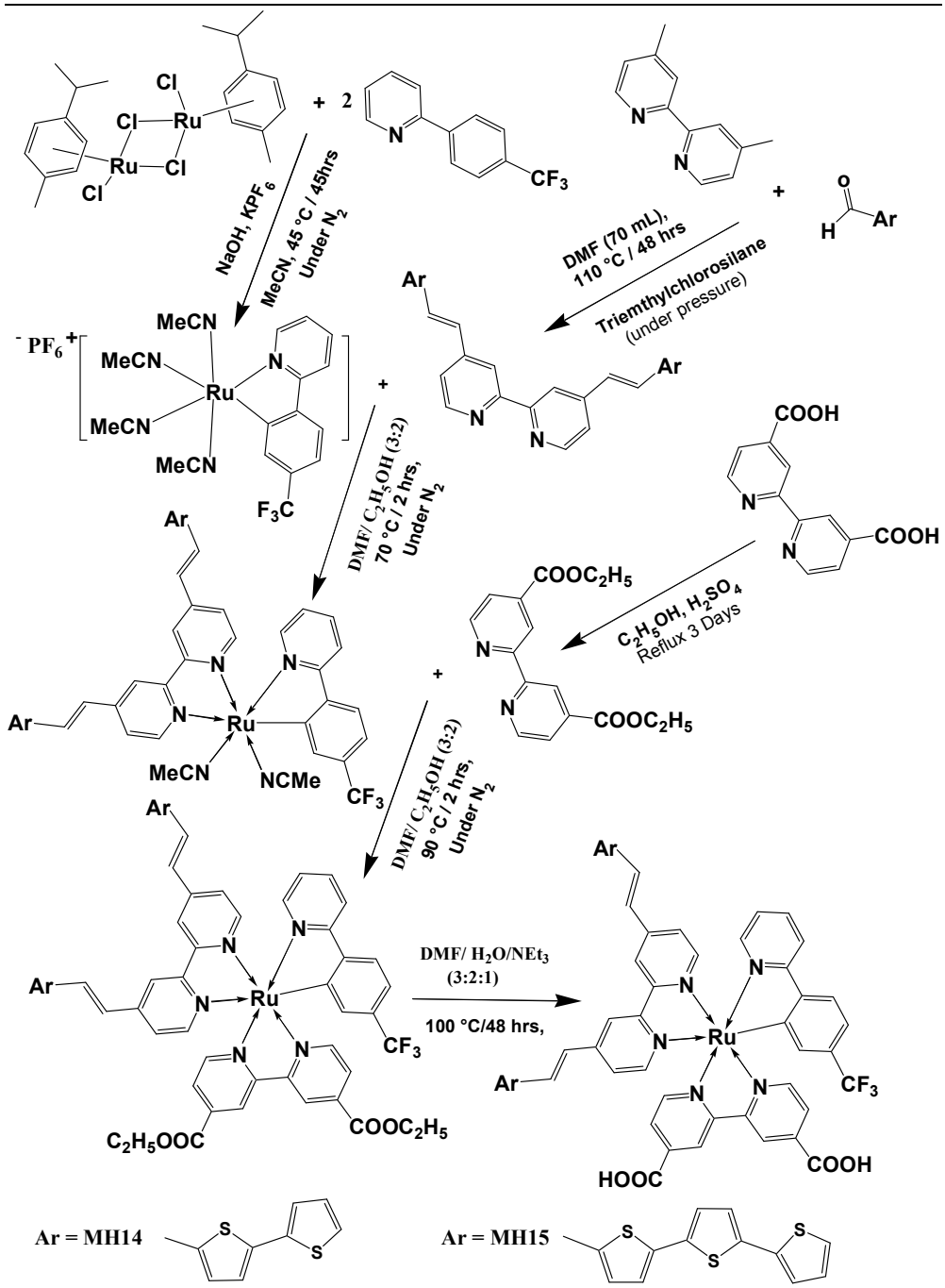

Scheme 1 General route for the synthesis of ligands and complexes MH14-15

Ru (II) cis[4,4'-Bis-(2-[2,2';5',2'']terthiophen-5-yl-vinyl)-[2,2']bipyridinyl-2, 2'-bipyridinyl-4, 4'-dicarboxylic-(2-(2,4-Difluoro-phenyl)-pyridine)] (MH15) complexes were prepared and purified using same procedure in 73% crude yield.

^{1}H-NMR, MH12 (500 MHz, DMSO-d6, 40 °C): δ/ppm 6.68 (d, 2H, *J* = 16.5 Hz and 7.54 (d, 2H, *J* = 7.07 Hz, CH=CH), 7.00-7.12 (m, 6H, Thio-H) 7.15 (t, 2H, *J* = 6.6 & 5.8 Hz Thio-H), 7.19 (d, 2H, *J* =7.6 Hz, Thio-H), 7.38 (d, 2H. *J* = 5.4 Hz ArH), 7.90 (d, 2H, *J* = 5.7 Hz, ArH), 8.84 (s, 2H, ArH), 9.08 (d, 2H, *J* = 8.2 Hz, ArH), 9.04 (s, 2H, ArH), 9.42 (d, 2H, *J* = 7.9 Hz ArH). **ESI-Mass:** Mass 997.95397; [M - 2H + TBA] $^{-1}$; Theo. M/Z = 1238.2231, Found. M/Z 1238.2222, Error = - 0.72 ppm. **FT-IR (ATR):** 2101 cm^{-1} (-NCS stretch, N-bonded isomer, very strong); 1717 cm^{-1} (C=O stretch of -COOH)

^{1}H-NMR, MH13 (500 MHz, DMSO-d6, 40 °C): **^{1}H-NMR, MH12** (700 MHz, DMSO-d6, 40 °C): δ/ppm 6.85 (d, 2H, *J* = 22.4 Hz and 7.55 (d, 2H, *J* = 7.0 Hz, CH=CH), 7.00-7.50 (m, 14H, Thio-H), 7.53 (d, 2H, *J* = 6.58 ArH), 7.62 (d, 2H, *J* =80 Hz, ArH), 8.23 (d, 2H. *J* = 6.8 Hz ArH), 8.50 (s, 2H, ArH), 9.09 (d, 2H, *J* = 7.8 Hz, ArH), 9.43 (s, 2H, ArH), 13.60 (s, 2H, v. weak, -COOH). **ESI-Mass:** Mass 1161.9294, [M – 2H + TBA] $^{-1}$, Theo. M/Z = 1402.1985, Found M/Z = 1402.1988, Error = -0.21ppm. **FT-IR (ATR):** 2101 cm^{-1} (-NCS stretch, N-bonded isomer, very strong); 1721 cm^{-1} (C=O stretch of -COOH)

^{1}H-NMR, MH14 (500 MHz, DMSO-d6, 40 °C): δ/ppm 6.99 (d, 2H, CH=CH), 7.01 (d, 2H, ArH), 7.08 (d, 2h, CH=CH) 7.13-7.17 (m, 8H, Thio-H); 7.33-7.37 (m, 2H, Thio-H); 7.40 (d, 2H, Hz, ArH), 7.51-7.61 (m, 4H, ArH), 7.90 (d, 2H, ArH), 7.93 (d, 1H, ArH), 7.98 (s, 2H, ArH), 8.26 (d, 2H, ArH), 8.88 (d, 2H, ArH), 8.99 (s, 2H, ArH). **FT-IR (ATR):** 1718 cm^{-1} (C=O stretch of -COOH), 1312 cm^{-1} (Ar-C-F, stretch)

^{1}H-NMR, MH15 (500 MHz, DMSO-d6, 40 °C): δ/ppm 7.16 (d, 2H, CH=CH), 7.17 (d, 2H, ArH), 7.21 (d, 2H, CH=CH) 7.20-7.23 (m, 12H, Thio-H); 7.54-7.55 (m, 2H, Thio-H); 7.41 (d, 2H, Hz, ArH), 7.49 (d, 2H, Hz, ArH); 7.84 (d, 2H, Hz, ArH); 7.90-7.93 (m, 2H, ArH), 7.97-7.99 (m, 2H, ArH), 8.07 (d, 1H, ArH), 8.38 (d, 2H, ArH), 9.12 (d, 2H, ArH), 9.21 (s, 2H, ArH). **FT-IR (ATR):** 1709 cm^{-1} (C=O stretch of -COOH), 1314 cm^{-1} (Ar-C-F, stretch)

2.2. Nanosecond Laser Flash Photolysis Spectroscopy:

An Edinburgh nanosecond laser flashphotolysis spectrometer (LP920) was used along with a Continuum Nd-YAG laser (Surelite; 10 Hz repetition rate; FWHM 5 ns) through a Surelite optical parametric oscillator (OPO). The output of the OPO was tuned at λ=430 nm. The beam was expanded by a planoconcave lens in order to irradiate the sample at a large cross section (more than 1 cm^2). The samples were oriented at 45 angle to both excitation and probe beams. Transparent mesoporous TiO_2 samples (thicknesses 6-12 μm) coated on glass substrates were dyed by adsorption of the **MH12-MH15** and **N719** complexes overnight. Two drops of LiI/I_2 electrolyte were sandwiched between the samples and a thin microscope cover glass. The samples were immediately subjected to some few tens of mJ/cm^2 of laser. Lower laser energies were avoided because it requires greater number of shots over a long period of time, which could lead to an early evaporation of electrolyte. For that reason, we kept the same conditions of high laser energies for all experiments. The transient absorption spectra of the specimen were recorded at probe light wavelength of λ=577 nm, where the ground state bleaching of the dye occurs.

3. Results and Discussions

UV-Visible and Emission Properties

Figure 3 illustrates the absorption and emission spectra of **MH12-15** versus **N719**, measured in DMF using concentration of 2 x10^{-5} M.

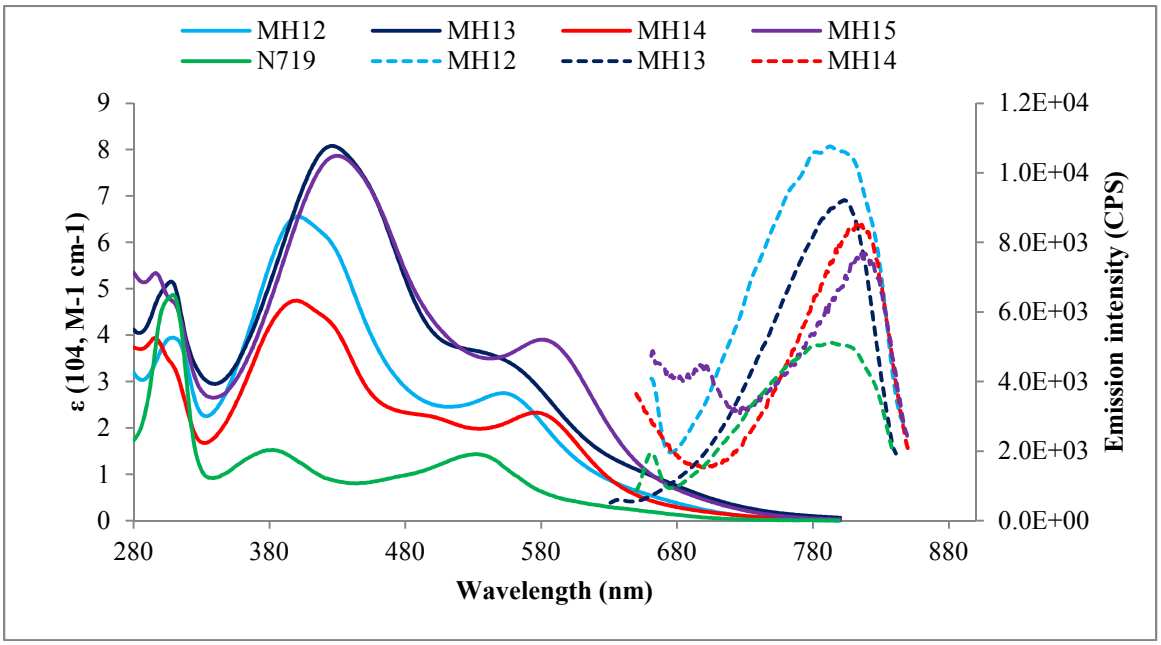

Figure 3: UV-Vis absorption spectra of complexes **MH12-15** compared to **N719**, measured in DMF (2 x10^{-5}M).

All four complexes showed bathochromic shift and higher intense MLCT absorption bands in the visible region than that of **N719.** This can be attributed to the strong electron-donor ability of the ancillary ligands of bi- and terthiophene. In the cyclometallated complexes **MH14-15**, the light harvesting efficiency was significantly red shifted compared to that of thiocynonated (-NCS) complexes **MH12-13.** This can be attributed to the fact that the incorporation of cyclometallated ligand (σ-donating ligand) destabilized the metal based HOMO more than that of ligand based LUMO by increasing the electron density on the metal center. As a result, the overall HOMO-LUMO gap decreased considerably, which translated into a significant red shift in the absorption spectra [19, 24-25]. Figure 4 illustrates the changes in energy levels upon introduction of a cyclometallated center.

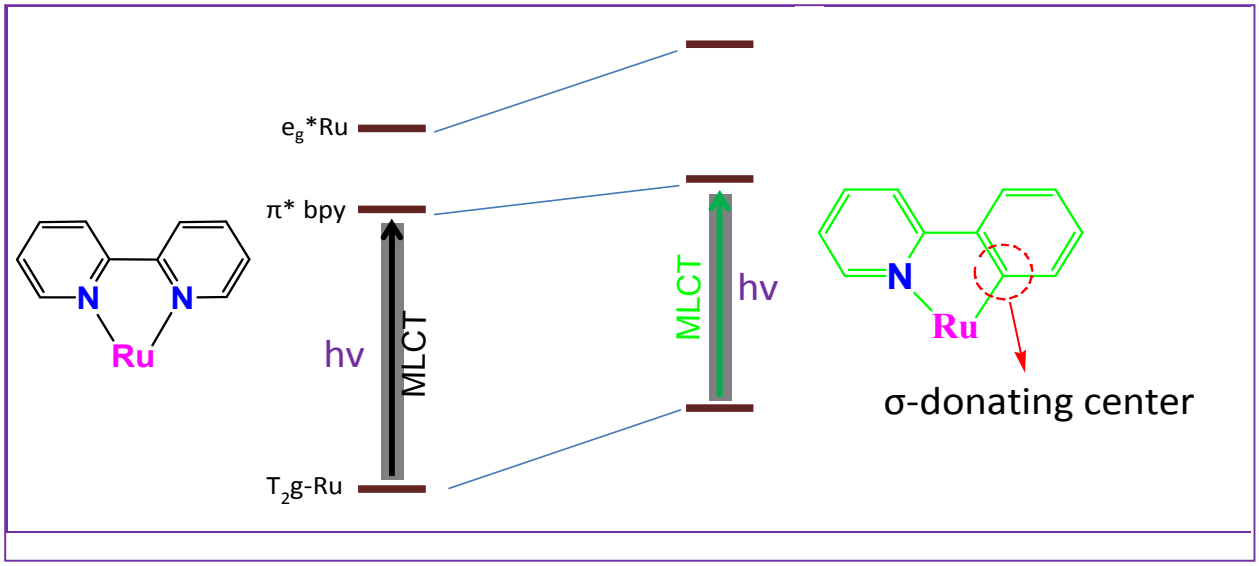

Figure 4: A schematic diagram of metal-to-ligand charge transfer (MLCT) in cyclometallating ligands that destabilizes the t_2g of Ru (II) as a result the HOMO-LUMO gap decreases. The σ-donating destabilized the metal-HOMO more than that of ligand-LUMO by transferring electron density into the metal center and imparts bathochromic shift in UV-Vis spectra.

MH12-13 showed lower energy MLCT at 553nm (27,500 $M^{-1}cm^{-1}$), 554nm (34,605 $M^{-1}cm^{-1}$), respectively, while in the cyclometallated complex **MH14-15**, the lower energy MLCT appeared at 577nm (23,300 $M^{-1}cm^{-1}$), 582nm (39,000 $M^{-1}cm^{-1}$), which confirms their superior light harvesting efficiency compared to **N719 (**530 nm, 14, 200 $M^{-1}cm^{-1}$). This remarkably high molar extinction coefficient can be attributed to the strong electron donating ligand and extended conjugation of the thiophene units coupled with one cyclometallation center. The UV-Vis absorption and emission results of **MH12-15** are summarized in Table 1. The emission was measured in the steady state mode by exciting at the lower energy MLCT band (λ_{max}) for each dye.

Table 1 Absorption and emission properties for **MH12-15** against **N719**

Complexes	Expt.[a] Absorption Spectrum (2x 10^{-5}mole)		Emission[b]
	λ_{max} (nm)	**ε (M^{-1} cm^{-1})**	$\lambda_{em\ (nm)}$
MH12	402; **553 (d→π*)**	65550; **27500**	796
MH13	427; **554 (d→π*)**	80800; **34605**	803
MH14	400; **577 (d→π*)**	47450; **23300**	806
MH15	431; **582 (d→π*)**	78650; **39000**	812
N-719	381; **530 (d→π*)**	14,400; **14,200**	746

[a] UV-Vis spectra measured in DMF (2x 10^{-5}M); [b] The emission spectra were obtained by exciting at the lowest MLCT band in DMF at 298K.

The UV-Vis spectral profiles of **MH12-15** when anchored on TiO_2 are significantly different from that in solution. The solution spectra in DMF solution gave two clear MLCT peaks in the visible region. However, on anchoring to TiO_2, both higher and lower energy MLCT in the visible region are overlapped to produce a broad absorption band covering the range 350nm extended into the near IR with the cut off at 800nm (Figure 5).

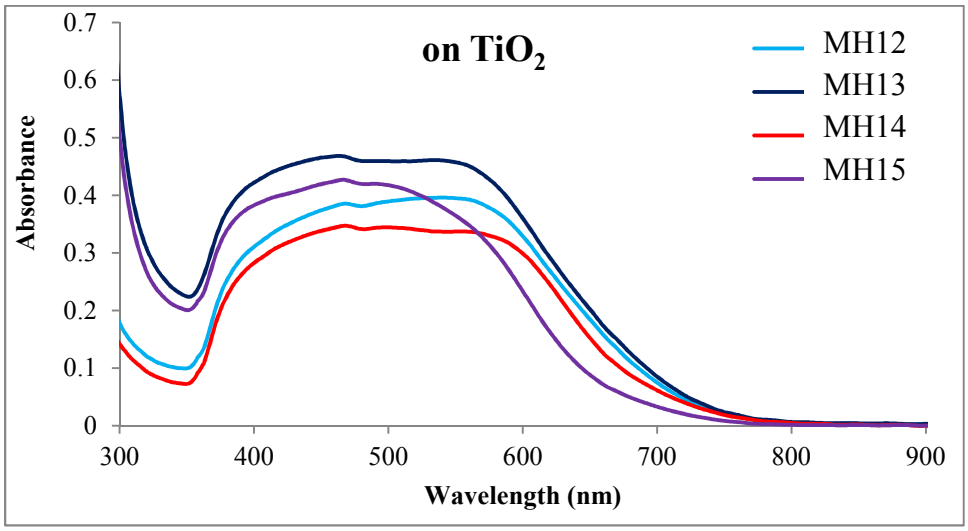

Figure 5: UV-Vis absorption spectra of complexes **MH12-15** anchored ontoTiO_2.

Ground and Excited State Potentials Properties

The ionization potential (IP), ground state oxidation potential (GSOP), of **MH12-15** anchored to TiO_2 film was measured using a photoemission yield spectrometer (Riken Keiki AC-3E), and the results are summarized in Table 2. The excited state oxidation potential (ESOP) of **MH12-15** and **N719** were estimated by subtracting the energy corresponding to lowest electronic transition ($E_{0\text{-}0}$) from the ground state oxidation potential (GSOP) while neglecting the reorganization of geometry and energies on the excited state [28], according to Equations (1).

$$\text{ESOP} = (G° - G^{+})_{ES} \approx (G° - G^{+})_{GS} - E_{0\text{-}0} \qquad (1)$$

and/or

$$\text{ESOP} = \text{GSOP} - E_{0\text{-}0}$$

The $(G° - G^{+})_{ES}$ and $(G° - G^{+})_{GS}$ are the free energy difference between the neutral and oxidized species at excited and ground states, respectively.

The experimental ionization potentials values for **MH12-15** and **N719** were -5.56, -5.51, -5.44, -5.36 and -5.76 eV. The IP values confirmed that the energy difference of the $Ru^{3+/2+}$ species of **MH12-13** are significantly below the redox potential of I_3^-/I^- (-5.2eV), confirming that there is enough thermodynamic driving force for dye regeneration. On the other hand, in **MH14-15**, the thermodynamic driving force of dye regeneration were only 0.24eV and 0.16eV, respectively, which is not sufficient driving forces for the efficient regeneration of neutral dyes, which led to inferior photovoltaic performance.

The experimental excited-state oxidation potentials E^* ($Ru^{3+/*}$) of **MH12-15** and **N719** are -3.70, -3.66, -3.67, -3.58 and -3.77eV, respectively, which lay above the conduction band edge of TiO_2 (-4.2 eV) [30], confirming efficient electron injection from the excited state of dye-sensitizer into the conduction band edge of TiO_2. A schematic interrelationship between ESOP, GSOP of **MH12-15** and **N719** against TiO_2 and I_3^-/I^- redox are illustrated in Figure 6.

Table 2 shows the excited state oxidation potential ($Ru^{3+/*}$), and the lowest singlet-singlet electronic transitions ($E_{0\text{-}0}$) for **MH12-15** compared to **N719.**

Complexes	Experimental (eV)		
	$^{*}E_{0\text{-}0}$	$^{\blacktriangledown}$IP (HOMO)	E^{*} ($Ru^{3+/*}$)
MH12	*1.85	-5.56	-3.71
MH13	*1.82	-5.51	-3.69
MH14	*1.77	-5.44	-3.67
MH15	*1.78	-5.36	-3.58
N719	*1.99	-5.76	-3.77

Excited state oxidation potential= ESOP =E^{*} ($Ru^{3+/*}$); $ESOP_{singlet}$= $-E_{HOMO}$ - $E_{0\text{-}0}$; $E_{0\text{-}0}$ = (S_0-S_1) = the lowest vertical excitation energy = the lowest singlet-singlet transition; GSOP = ground state oxidation potential= E_{HOMO}; $^{*}E_{0\text{-}0}$=based on the experimental absorption and emission spectra (DMF), calculated from the point of overlap. $^{\blacktriangledown}$IP= $Ru^{3+/2+}$=GSOP= The ionization potential measured using a photoemission yield spectrometer (Riken Keiki AC-3E); Exited-state oxidation potential, E^{*} ($Ru^{3+/*}$), was calculated from: E^{*} ($Ru^{3+/*}$) = $Ru^{3+/2}$ - $^{*}E_{0\text{-}0}$. Calculated HOMO, ESOP, and $E_{0\text{-}0}$ of N719 were performed elsewhere.[28]

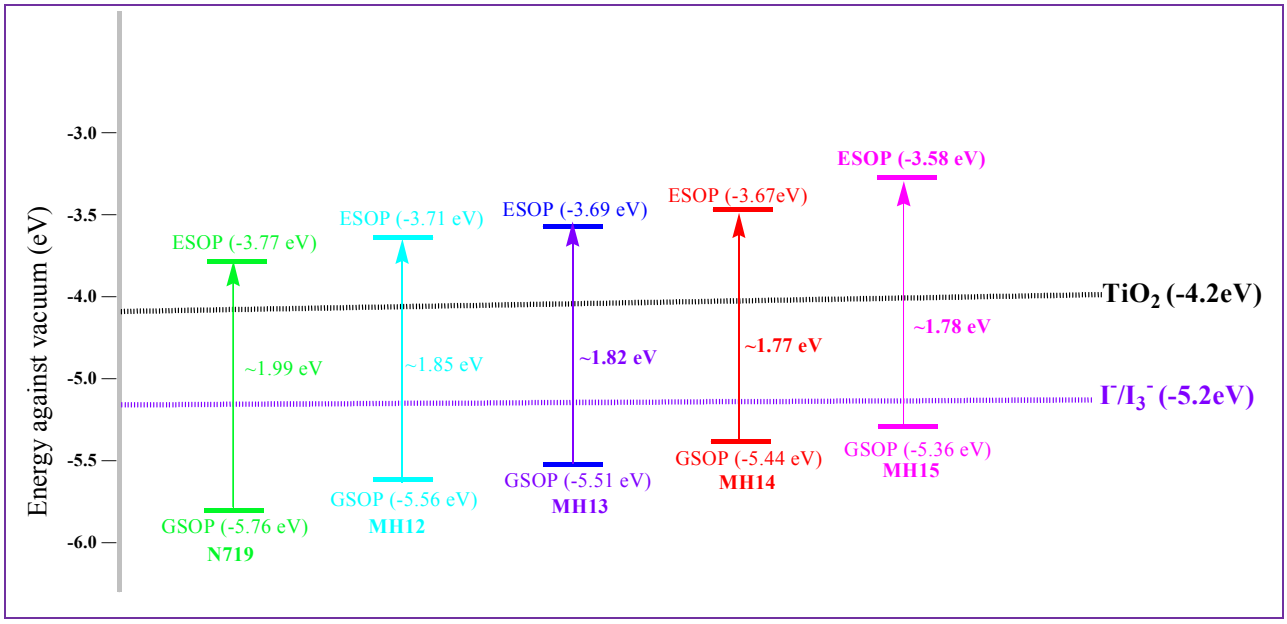

Figure 6 A schematic interrelationship between experimental ground (GSOP, $Ru^{3+/2+}$) and excited state oxidation potential (ESOP =E^{*} ($Ru^{3+/*}$), HOMO-LUMO gape ((S_0-S_1) of **MH12-15** and **N719** with respect to **TiO_2** and **I/I_3^-** redox couple.

Photovoltaic Device Characterization

The photovoltaic performance of complexes **MH12-14** against **N719** on nanocrystalline TiO_2 electrode was studied under standard AM 1.5 irradiation (100 mW cm^{-2}). The incident-photon-to-current efficiency conversion (IPCE) spectra are plotted as a function of wavelength shown in Figure 7.

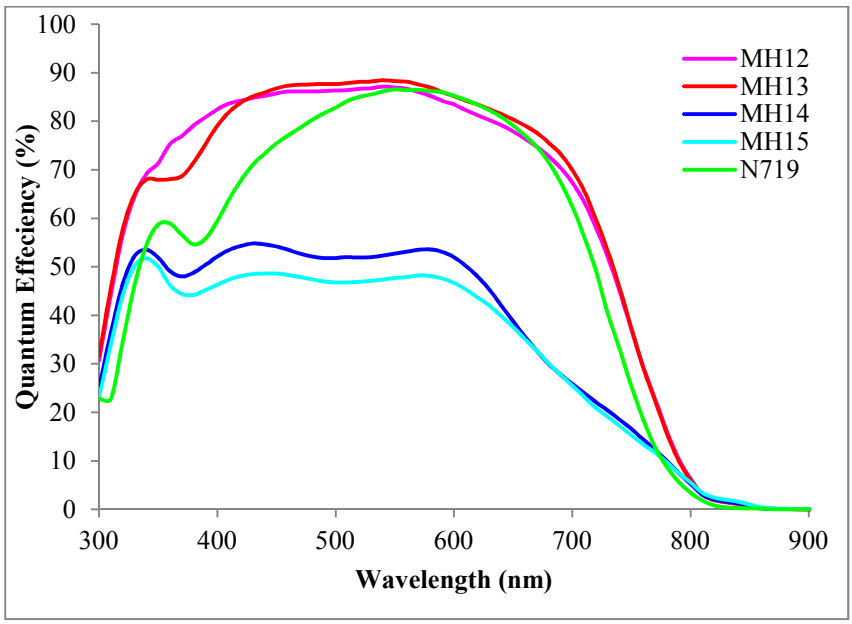

Figure 7: Photocurrent action spectra of **MH12-15**, [a] conditions: sealed cells; coadsorbate, DCA 20 mM; photoelectrode, TiO_2 (15 µm thickness and 0.25 cm^2); electrolyte, 0.6 M DMPII, 0.1 M LiI, 0.05 I_2 in AN; irradiated light, AM 1. 5 solar light (100 mW cm^{-2})

The IPCE spectra of solar device containing **MH12-13** demonstrated the most efficient sensitization over broad wavelength range including the entire visible and extended into the near IR region (ca. 830 nm). The IPCE value is over 85% in the plateau region. Despite the impressive molar extinction coefficient of both cyclometallated complexes **MH14-15,** they exhibited inferior IPCE values, which can be attributed to poor dye regeneration.

The photovoltaic characteristics of **MH12-15** and **N719** were studied using electrolytes with 0.0M, 0.3M or 0.5M of 4-tert-butylpyridine (TBP) used as an additive. The photovoltaic parameters including the short-circuit photocurrent density (J_{SC}), open-circuit voltage (V_{OC}), fill factors (*FF*) and overall cell efficiencies (η) for each solar cell were measured, and the results are summarized in Table 3 and Figure 8.

Table 3 Photovoltaic performance of Ru (II) complexes **MH12-15** against **N719**

Complexes	TBP (M)	J_{sc}(mA cm^{-2})	V_{oc} (V)	FF	η (%)
MH12	0.3	20.454	0.630	0.686	8.83
	0.5	19.140	0.653	0.698	8.72
MH13	0.3	20.585	0.660	0.715	9.71
	0.5	19.872	0.676	0.716	9.62
MH14	0.0	16.999	0.492	0.642	5.37
	0.3	12.832	0.584	0.647	4.85
MH15	0.0	14.68	0.497	0.614	4.48
	0.3	10.787	0.575	0.682	4.23
N719	0.3	17.16	0.733	0.725	9.12
	0.5	16.85	0.749	0.739	9.32

[a] Conditions: sealed cells; coadsorbate, DCA 20 mM; photoelectrode, TiO_2 (15 μm thickness and 0.25 cm^2); electrolyte, 0.6 M DMPII, 0.1 M LiI, 0.05 I_2 in AN; irradiated light, AM 1. 5 solar light (100 mW cm^{-2}). J_{SC}, short-circuit photocurrent density; V_{oc}, open-circuit photovoltage; FF, fill factor; η, total power conversion efficiency.

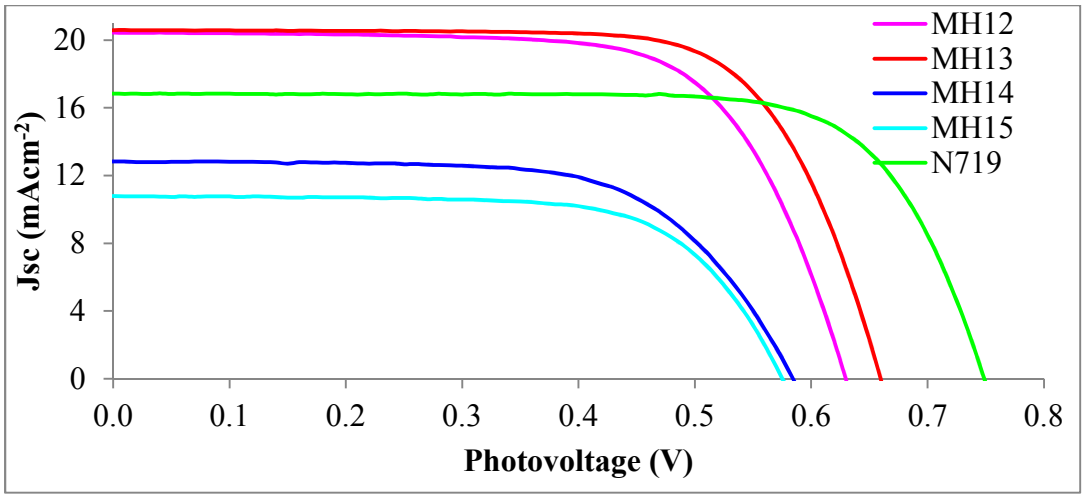

Figure 8 Photocurrent voltage characteristics of DSSCs sensitized with the complexes **MH12-15** against **N719**. Electrolyte, 0.6 M DMPII, 0.1 M LiI, 0.05 I_2 in acetonitrile (AN).

Among the series of the named dyes, **MH13** demonstrated the best DSSCs performance showing short-circuit photocurrent density of 20.58 $mAcm^{-2}$, an open-circuit photovoltage of 0.660 V, and a fill factor of 0.715, corresponding to an overall conversion efficiency (η) of 9.71%. The J_{sc} values of **MH12** (20.45 mA cm^{-2}) is comparable to **MH13** and still considerably higher than that of **N719 (**17.16 mA cm^{-2}), which can be attributed to the better light harvesting efficiency throughout the visible region and NIR region up to 830nm. However, the overall conversion efficiency of **MH12** (8.83%) is lower than that of **N719 (**9.32%) which is attributed to poor charge separation (V_{oc}) at the interface of dye/TiO_2/electrolyte and/or recombination reactions at the interfaces of TiO_2/dye/electrolyte. The V_{oc} and FF of **MH13** is higher than that of **MH12**, which can be attributed to the larger molecular size and higher molar extinction coefficient of the former, which translates into less dye on thinner film of TiO_2, and that could facilitate more charge collection and a reduction in dark current and enhanced performance of DSSCs. However, inferior photovoltaic performance was observed for **MH14** and **MH15** in both photocurrent and photovoltage, which can be attributed to the weak thermodynamic driving force of 0.24 and 0.16eV, respectively, of neutral dye regeneration.

Excited and Ground States Dynamics

In order to scrutinize the dynamics of dye regeneration of **MH12-15** by the electrolyte, we performed nanosecond time-resolved laser experiments of the TiO_2/dye/-electrolyte interface. Transient absorbance measurements shown in Figure 9 monitor directly the time needed for different oxidized dyes to regenerate the neutral dye by a reduction process from LiI/I_2 redox species present in electrolyte, and this experiment was performed in comparison with N719 dye regeneration time under the same experimental conditions. Complexes **MH12** and **MH13** showed comparable lifetime decay for dye regeneration of 6 μs and 4 μs, respectively, compared to N719 (2.3 μs) [32]. This could be one of the mains reasons why **MH12** and **MH13** achieved significantly higher photocurrent. Under the same experimental device conditions, **MH14** and **MH15** showed slower dye regeneration decay lifetimes of 13 μs and 18 μs, respectively, which explain the inferior photocurrent performance of these dyes. Based on results presented in Figure 6, compared to the energy values of the GSOP of **MH12** and **MH13** with respect to the redox potential of the electrolyte, complexes **MH14** and **MH15** exhibited much less thermodynamic driving force for electron replenishment to generate the neutral dye. Hence, it can be confirmed that the low driving force for **MH14** and **MH15** is most likely the main reason for the inferior short-circuit photocurrent density observed.

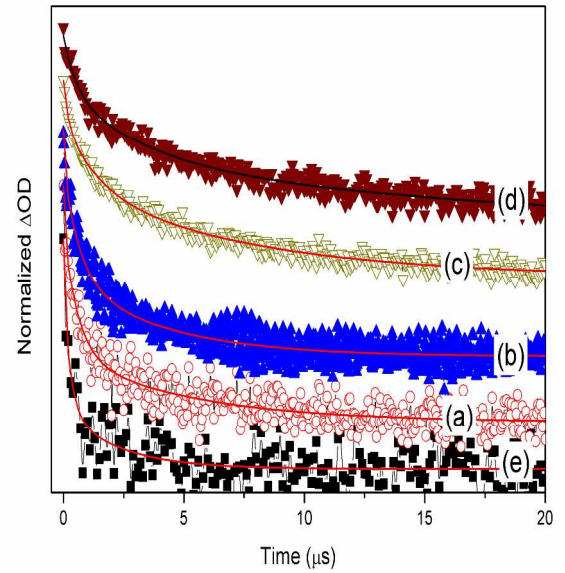

Figure 9 Transient absorbance decay profiles obtained upon nanosecond pulsed laser excitation at λ=430 nm (for MH dyes) and λ=430 nm (for N719 dye), in presence of LiI/I_2 electrolyte of mesoporous TiO_2 films sensitized with, (a) MH12; (b) MH13; (c) MH14; (d) MH15 and (e) N719.

Conclusions

The incorporation of cyclometallated ligand in Ru (II) polypyridyl moiety (**MH14-15**) produced considerable red-shift of 24nm and 28nm in the low energy MLCT compared to those of non-cyclometallated analogues **MH12-13**, respectively. Despite impressive molar extinction coefficient and red shift in **MH14-15**, they exhibited inferior photovoltaic performance because the thermodynamic drive forces of dye regeneration **MH14-15** were less than 0.25eV, which demonstrates clearly that the driving force of dye regeneration must be at least 0.25eV. Furthermore, it was demonstrated, using nanosecond transient absorbance measurements, that the time needed for the oxidized forms of **MH12-MH15** to regenerate the neutral dye by gaining an electron from the electrolyte is 6 μs, 4 μs, 13 μs and 18 μs, respectively, compared to N719 (2.3 μs). These data confirmed that the weak thermodynamic force, small negative free energy (-ΔG), for neutral dye regeneration of **MH14-15** makes the dye regeneration process kinetically sluggish, which contributed significantly to the loss of photocurrent and photovoltage. Among **MH12-15**, it was also shown that **MH13** achieved the best photovoltaic performance, and it outperformed **N719** by 58% in molar absorptivity, 17% in photocurrent, and 6% in total conversion efficiency under the same experimental device conditions. Therefore, fine tuning of the HOMO of **MH14-15** coupled with their inherent superior light harvesting capabilities could lead to a novel generation of superior panchromatic sensitizers that may exceed 12% total conversion efficiency.

References

1. Hardin, B. E.; Snaith, H. J.; Michael D. McGehee, M. D. *Nature photonics* **2012,** *6,* 162.

2. Qin, Y.; Q., P. *International Journal of Photoenergy* **2012,** *2012,* 1.

3. Kuang, D.; Klein, C.; Ito, S.; Moser, J. E.; Baker, R. H.; Evans, N.; Duriaux, F.; Gräetzel, C.; Zakeeruddin, S. K.; Gräetzel, M. *Adv. Mater* **2007,** *19,* 1133.

4. Kohle, O.; Gratzel, M. *Advanced Materials* **1997,** *9,* 904.

5. Bomben, P. G.; Gordon, T. J.; Schott, E.; Berlinguette, C. P. *Angew. Chem. Int. Ed.* **2011,** *50,* 10682.

6. Isalm, A.; Singh, S. P.; Yanagida, M.; Karim, M. R.; Han, L. *Intternational Journal of Photochemistry* **2010,** *2011 ,* 7.

7. Hagfeldt, A.; Boschloo, G.; Sun, L.; Kloo, L.; Pettersson, H. *Chemical Review* **2010,** *110,* 6516.

8. Gao, F.; Wang, Y.; Shi, D.; Zhang, J.; Wang, M.; Jing, X.; Baker, R. H.; Wang, P.; Zakeeruddin, S. M.; Gräetzel, M. *J. Am. Chem. Soc.* **2008,** *130,* 10720.

9. Shi, D.; Pootrakulchote, N.; Li, R.; Guo, J.; Wang, Y.; Zakeeruddin, S. M.; l Gräetzel, M.; Wang, P. *J. Phys. Chem. C* **2008,** *112,* 17046.

10. Yum, J. H.; Jung, I.; Baik, C.; Ko, J.; Nazeeruddin, M. K.; Gräetzel, M. *Energy Environ. Sci.* **2009,** *2,* 100.

11. Jiang, K. J.; Masaki, N.; Xia, J. B.; Noda, S.; Yanagida, S. *Chem. Commun.* **2006,** 2460.

12. Yu, Q.; Liu, S.; Zhang, M.; Cai, N.; Wang, Y.; Wang, P. *J. Phys. Chem. C,* **2009,** *113,* 14559.

13. Chou, C. C.; Wu, K. L.; Yun, C.; Hu, W. P.; Yu, S. J. *Angew. Chem. Int.Ed.* **2011,** *50,* 2054.

14. Bomben, P. G.; Koivisto, B. D.; Berlinguette, C. P. *Eur. J. Inorg. Chem.* **2011,** *11,* 1806.

15. Asghar, M. I.; Miettunen, K.; Haleme, J.; Vahermaa, P.; Toivola, M.; Lund, P. *Energy Environ. Sci.* **2010,** *3,* 418.

16. Gräetzel, M. *Journal of Photochemistry and Photobiology C: Photochemistry Reviews* **2003,** *4,* 145.

17. Gräetzel, M. *Inorg. Chem.* **2005,** *44,* 6841.

18. Bomben, P. G.; Robson, K. C. D.; Koivist, B. D.; Berlinuett, C. P. *Coordination Chemistry Reviews* **2012,** *256,* 1438.

19. Barigelletti, F.; Ventura, B.; Collin, J. P.; Kayhanian, R.; Gavina, P.; Sauvage, J. P. *Eur. J. Inorg. Chem* **2000,** 113.

20. Wadman, S. H.; Kroon, J. M.; Bakker, K.; Lutz, M.; Spek, A. L.; Klink, G. P.; Koten, G. *Chem. Commun.* **2007,** 1907.

21. Bessho, T.; Zakeeruddin, S.; Yeh, C. Y.; Diau, E. G.; Gräetzel, M. *Angew. Chem., Int. Ed.* **2010,** *49,* 6646.

22. Zeng, W.; Cao, Y.; Bai, Y.; Wang, Y.; Shi, Y.; Zhang, M.; Wang, F.; Pan, C.; Wang, P. *Chem. Mater.* **2010,** *22,* 1915.

23. Wu, K. L.; Hsu, H.-C.; Chen, K.; Chi, Y.; Chung, M.-W.; Liu, W.-H.; Chou, P.-T. *Chem. Commun.* **2010,** *46,* 5124.

24. Constable, E.; Thompson, A.; Cherryman, J.; Liddiment, T. I. *Chim. Acta.* **1995,** *235,* 156.

25. Barigelletti, F.; Ventura, B.; Collin, J.; Kayhanian, R.; Gavina, P.; J.P., S. *Eur. J. Inorg. Chem.* **2000,** 113.

26. El-Shafei, A., Hussain, M., Atiq, A., Islam, A,. Han, L. *J. Mater. Chem.* ***2012****, 22, 24048.*

27. Nazeeruddin, Md. K.; Zakeeruddin, S. M.; Humphry-Baker, M. J.; Liska, P.; Vlachopoulos, V. S.; Fischer, C.-H.; Gräetzel, M. *Inorg. Chem.* **1999**, *38*, 6298.

28. De Angelis, F.; Fantacci, S.; and Sellon, A., Nanotechnology, **2008**, 19, 424002.

29. Oskam, G.; Bergeron, B. V.; Meyer, G. J.; and Searson, P. C., J. Phys. Chem. B **2001**, 105, 6867.

30. Hagfeld, A.; Gräetzel, M., Chem. Rev. **1995**, 95, 49.

31. Sauvage, F.; Fischer, M, R.; Mishra, A.; Zakeeruddin, S, M.; Nazeeruddin, M, K.; Buerle, P.;

Gräetzel, M., *ChemSusChem,* 2009, 2, 761.

32. Wang, P.; Zakeeruddin, S. M.; Moser, J. E.; Nazeeruddin, M. K.; Sekiguchi, T.; and Gräetzel, M. A stable quasi-solid-state dye-sensitized solar cell with an amphiphilic ruthenium sensitizer and polymer gel electrolyte, *Nature Materials* 2, 402–407 (2003).

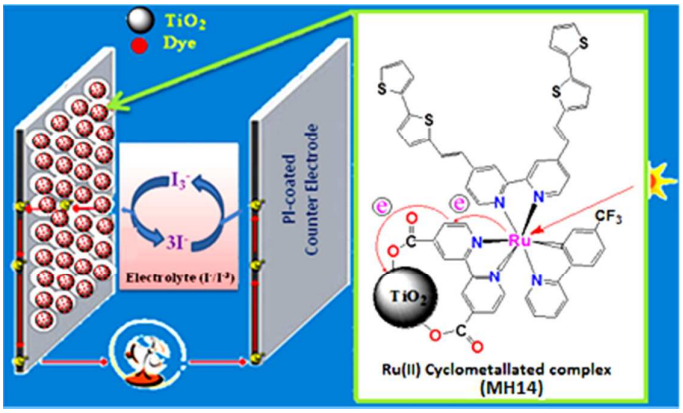

Four novel Ru (II) bipyridyl complexes were synthesized and characterized for dye-sensitized solar cells (DSSCs). Although cyclometallation may produce significantly better light harvesting, a driving force < 0.25 eV is not sufficient for effective dye regeneration.